JOURNAL OF GUIDANCE, CONTROL, AND DYNAMICS
Vol. 30, No. 2, March–April 2007

Differential Semimajor Axis Estimation Performance Using Carrier-Phase Differential Global Positioning System Measurements

Jonathan P. How,* Louis S. Breger,† and Megan Mitchell‡
Massachusetts Institute of Technology, Cambridge, Massachusetts 02139-4307
Kyle T. Alfriend§
Texas A&M University, College Station, Texas 77843
and
Russell Carpenter‖
NASA Goddard Space Flight Center, Greenbelt, Maryland 20771

DOI: 10.2514/1.23083

This paper investigates the impact of navigation errors on the navigation and control aspects of formation flying spacecraft. The use of carrier-phase differential Global Positioning System measurements in relative navigation filters is analyzed, with a particular focus on the semimajor axis error. Semimajor axis error is shown to be the sum of two positive quantities that are related to the satisfaction of the *balance* and *correlation* requirements. Previous publications have suggested that a "good" navigation filter would yield estimates of the along-track velocity and radial position that are strongly correlated. However, practical experience with filters based on the carrier-phase differential Global Positioning System measurements has shown that this seldom occurs, even when the estimation accuracies are very good. Analytical methods and numerical simulations are used to show that the optimal semimajor axis estimate from a Kalman filter does not satisfy these requirements for any combination of measurement and process noise. Numerical examples with a fully nonlinear extended Kalman filter appear to bear out these conclusions. The combination of these simulations and analysis provides new insights on the crucial role of the process noise in determining semimajor axis knowledge.

I. Introduction

IN any space mission, accurate orbit predictions are often at least as important as accurate solutions at epoch. Accurate predictions are required for such purposes as acquisition, pointing, conjunction analysis, and maneuver planning. For problems such as rendezvous, formation flying, constellations, and debris avoidance, accurate predictions of the relative orbital motion may be even more significant. Because linearized two-body motion, which is unstable along the orbit track, is the dominant dynamic mode, the most significant means to achieve accurate prediction is to control absolute and/or relative along-track error growth. Minimizing along-track error growth for a Keplerian system (i.e., no atmospheric disturbances or Earth oblateness effects) requires accurate absolute and/or relative knowledge of the orbital energy [equivalently, period, semimajor axis (SMA), or mean motion], as well as accurate knowledge of the ratio of the radial and along-track components of orbital speed (equivalently, flight-path angle). These requirements constrain the ratios and, hence, correlations between errors in along-track position and radial velocity, as well as between errors in radial position and along-track velocity.

These relationships were recognized and documented for near-circular orbits at least as far back as the time of Apollo 8 [1] and were specified in terms of the components of the navigation error covariance matrix at least as early as 1987 [2]; the cited works, though publicly available, were not widely known, although the relationships themselves appear to have been widely known as industry folklore. Some of the first documented successful Global Positioning System (GPS) spaceflight experiments were found to not fully satisfy these constraints [3], and subsequent analysis of precise relative GPS navigation in the context of formation flying has demonstrated that increasing the GPS accuracy leads to similar conclusions [4,5]. This work presents simple analytical experiments to demonstrate that the Kalman filter does not satisfy the previously mentioned relationships, which are referred to here as the *correlation* and *balance* properties. In particular, it is shown that no combination of measurement noise and process noise in a simplified Kalman filter can achieve solutions that have previously been understood to generate accurate orbit predictions. Numerical examples with a fully nonlinear extended Kalman filter (EKF) appear to bear out these conclusions. This conclusion is reminiscent of experiences that the author of [6] claimed as his motivation for deriving a nonwhite process noise model based on gravity errors for sequential orbit determination. Reference [7] makes similar conclusions concerning physically connected bias models for drag. One contribution of the present work is to present a solid foundation for such empirical observations.

II. Background

In formation flying missions, accurate knowledge of the difference in semimajor axes or, equivalently, the difference in orbital energy between the vehicles in a formation is important [3–5,8]. A difference in semimajor axes means that the two vehicles have different orbital periods and thus they will drift out of formation

Presented as Paper 5024 at the AIAA Guidance, Navigation, and Control Conference and Exhibit, Providence, Rhode Island, 16–19 August 2004; received 8 February 2006; revision received 26 June 2006; accepted for publication 8 July 2006.

*Associate Professor, Department of Aeronautics and Astronautics; jhow@mit.edu.
†Research Assistant, Department of Aeronautics and Astronautics; lbreger@mit.edu.
‡Department of Aeronautics and Astronautics; megan.mitchell@alum.mit.edu.
§Professor, Department of Aerospace Engineering; alfriend@aero.tamu.edu.
‖Russell.Carpenter@nasa.gov.

unless regular control effort is applied [9]. The output of a carrier-phase differential GPS (CDGPS) Kalman filter includes the relative formation state in a local vertical local horizontal (LVLH) reference frame, where the radial, in-track, and cross-track directions define the x, y, and z axes. Understanding the relationship between position and velocity accuracies and semimajor axis accuracy is key to evaluating the output of this type of filter.

Although [4] develops the navigation error analysis from absolute state relations, the results can be reformulated for the relative case. The relative navigation error equations, shown next, relate semimajor axis error to position and velocity errors. Note that this discussion is limited to circular reference orbits. The semimajor axis a of vehicle i is

$$\frac{1}{a_i} = \frac{2}{r_i} - \frac{v_i^2}{\mu} \tag{1}$$

where r and v are the radius and speed in the Earth-centered inertial (ECI) reference frame, and μ is the gravitational constant of the Earth. Equation (1) is used to find the difference in semimajor axes of vehicles i and j:

$$\Delta a_{ij} \approx 2(r_j - r_i) + (2/n)(v_j - v_i) \tag{2}$$

where one vehicle is assumed to be in a near-circular orbit and the other within close proximity.

The approximate change in the semimajor axis is caused by a difference in the two radii and the two velocity magnitudes. To first order, the difference in the magnitude of two close vectors is caused by the difference in length along the vector. Consequently, for the relative position vectors, this magnitude difference is primarily due to the difference in radii, and for the relative velocities, the difference in along-track velocities. The relative dynamics in the LVLH reference frame are described by the Hill–Clohessy–Wiltshire (HCW) equations [10]:

$$\ddot{x} - 2n\dot{y} - 3n^2x = f_x \qquad \ddot{y} + 2n\dot{x} = f_y \qquad \ddot{z} + n^2 z = f_z \tag{3}$$

The force-free solution to the HCW equations is

$$\begin{aligned} x(t) &= \frac{\dot{x}_0}{n}\sin nt - \left(\frac{2\dot{y}_0}{n} + 3x_0\right)\cos nt + \left(\frac{2\dot{y}_0}{n} + 4x_0\right) \\ y(t) &= \frac{2\dot{x}_0}{n}\cos nt + \left(\frac{4\dot{y}_0}{n} + 6x_0\right)\sin nt + \left(y_0 - \frac{2\dot{x}_0}{n}\right) \\ &\quad - (3\dot{y}_0 + 6nx_0)t \\ z(t) &= z_0\cos nt + \frac{\dot{z}_0}{n}\sin nt \end{aligned} \tag{4}$$

Compensating for the Coriolis effect of differentiating in the rotating HCW reference frame, the difference in semimajor axes (the ij subscript is subsequently omitted) can be approximately written in terms of the relative radial position x and the in-track velocity $\dot{y}$, as

$$\Delta a \approx 2[2x + (\dot{y}/n)] \tag{5}$$

This expression for the differential semimajor axis applies throughout the orbit, but using Eq. (4), it can be rewritten as

$$\Delta a \approx -(3\dot{y} + 6nx)(-2/3n) = -(3\dot{y}_0 + 6nx_0)(-2/3n) \tag{6}$$

which shows that it is directly related to the secular drift term in the in-track solution to the HCW equations in Eq. (4). Clearly, if the difference in semimajor axes is zero, then there will be no secular drift between the spacecraft. This is the linearized form of the more general energy-matching condition, which is that spacecraft with equivalent semimajor axes will not drift apart. The standard deviation of the approximate differential semimajor axis estimate, $\sigma_{\Delta a}$, is given by [4]

$$\sigma_{\Delta a} = 2\sqrt{4\sigma_x^2 + (4/n)\rho_{x\dot{y}}\sigma_x\sigma_{\dot{y}} + (1/n^2)\sigma_{\dot{y}}^2} \tag{7}$$

The parameters σ_x, $\sigma_{\dot{y}}$, and $\rho_{x\dot{y}}$ are derived from the error covariance matrix for the relative LVLH state estimate:

$$\hat{\mathbf{x}} = [x \quad \dot{x} \quad y \quad \dot{y}]^T$$

with estimation error $\tilde{\mathbf{x}} = \hat{\mathbf{x}} - \mathbf{x}$, which is assumed to be unbiased, $E[\tilde{\mathbf{x}}] = \mathbf{0}$, and have a covariance

$$E[\tilde{\mathbf{x}}\tilde{\mathbf{x}}^T] = \begin{bmatrix} \sigma_x^2 & \rho_{x\dot{x}}\sigma_x\sigma_{\dot{x}} & \rho_{xy}\sigma_x\sigma_y & \rho_{x\dot{y}}\sigma_x\sigma_{\dot{y}} \\ \rho_{\dot{x}x}\sigma_{\dot{x}}\sigma_x & \sigma_{\dot{x}}^2 & \rho_{\dot{x}y}\sigma_{\dot{x}}\sigma_y & \rho_{\dot{x}\dot{y}}\sigma_{\dot{x}}\sigma_{\dot{y}} \\ \rho_{yx}\sigma_y\sigma_x & \rho_{y\dot{x}}\sigma_y\sigma_{\dot{x}} & \sigma_y^2 & \rho_{y\dot{y}}\sigma_y\sigma_{\dot{y}} \\ \rho_{\dot{y}x}\sigma_{\dot{y}}\sigma_x & \rho_{\dot{y}\dot{x}}\sigma_{\dot{y}}\sigma_{\dot{x}} & \rho_{\dot{y}y}\sigma_{\dot{y}}\sigma_y & \sigma_{\dot{y}}^2 \end{bmatrix} \tag{8}$$

Defining the *balance index* as

$$\texttt{bal} = \left|1 - \frac{2n\sigma_x}{\sigma_{\dot{y}}}\right| \tag{9}$$

then the semimajor axis standard deviation in Eq. (7) can be rewritten as

$$\sigma_{\Delta a} = 2\sqrt{\left(\frac{\texttt{bal}\cdot\sigma_{\dot{y}}}{n}\right)^2 + \frac{4\sigma_x\sigma_{\dot{y}}}{n}(1 + \rho_{x\dot{y}})} \tag{10}$$

This relationship makes it clear that the two conditions for zero semimajor axis standard deviation are: 1) correlation requirement $\rho_{x\dot{y}} = -1$, that is, the radial position and in-track velocity are linearly correlated and 2) balance requirement $\texttt{bal} = 0$ or, equivalently, that $\sigma_{\dot{y}} = 2n\sigma_x$.

Reference [4] proposed a method for representing the relationship between σ_x, $\sigma_{\dot{y}}$, $\rho_{x\dot{y}}$, and $\sigma_{\Delta a}$ that is illustrated in Fig. 1. The x and y axes of the plot are the standard deviations of the position and velocity estimation errors. Contours of constant semimajor axis standard deviation are shown on the figure. Each contour is associated with a value of $\rho_{x\dot{y}}$ in addition to a level of $\sigma_{\Delta a}$; several values of $\rho_{x\dot{y}}$ are shown for each level of $\sigma_{\Delta a}$. The diagonal of peaks indicates where $\sigma_{\dot{y}} = 2n\sigma_x$. Along the diagonal of peaks, the lines of constant semimajor axis experience a "bump" that increases in size as the correlation tends toward -1. This bump corresponds to increasing cancellation between the error in x and $\dot{y}$ that results from increasing correlation in these errors. Essentially, if the errors have high correlation and the proper balance, the higher error levels can be tolerated while maintaining low levels of semimajor axis error. Each point on the graph corresponds to a unique set of σ_x and $\sigma_{\dot{y}}$. However, many points on the graph are intersected by more than one contour of constant semimajor axis. The correlation determines the specific contour on which the system lies.

Remark 1: Figure 2 shows contours for a particular semimajor axis standard deviation error ($\sigma_{\Delta a} = 1$ m) for varying values of correlation. The plot also shows lines of constant balance index. Clearly, bal should be zero when the balance requirement is met. The plot shows that if the balance is off, that is, $\texttt{bal} \approx 0.5$ or $\texttt{bal} \approx |-1|$, then the effects of the correlation are reduced. This reinforces the observation that for systems governed by the HCW equations, both the correlation and balance requirements must be satisfied to obtain a significant reduction in the semimajor axis error. □

III. Detailed Filter Analysis

This section presents analytical relationships for a Kalman filter between the process and measurement noise levels and the SMA balance and correlation requirements. The link between the two is established using the algebraic Riccati equation. If they exist, analytic solutions to the Riccati equation provide insights into the effect of the parameters in the estimation problem, but these are typically very difficult to obtain for high-order systems. However, for a Kalman filter with a measurement update every $\Delta t \approx 1$ s for a 90-min orbit [11,12], the coupling between motion in the x and y directions is very weak and the dynamics can be well approximated as two weakly coupled double integrators. This section uses this

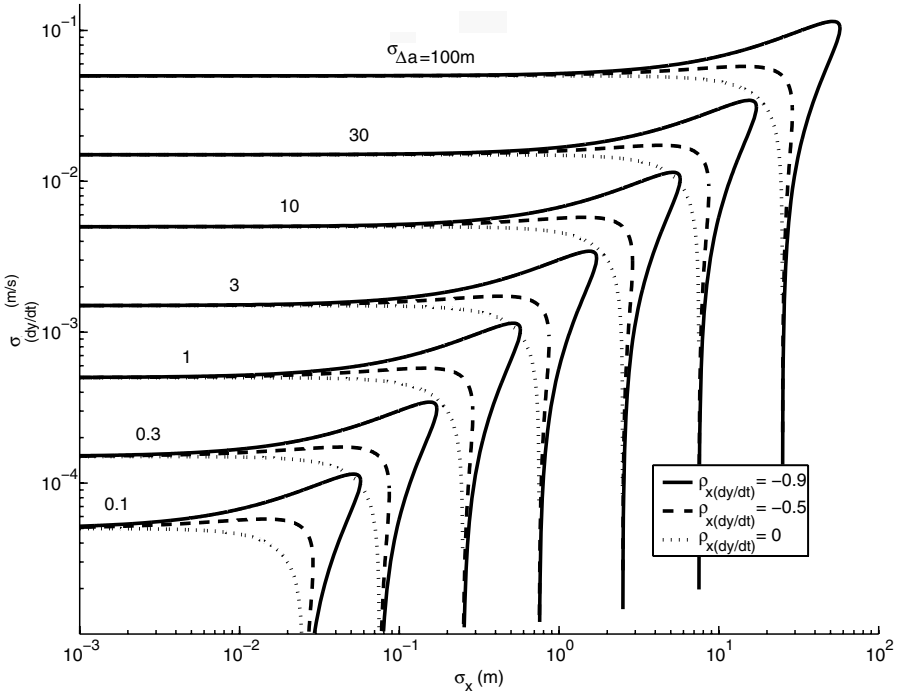

Fig. 1 Contours of constant semimajor axis vs position and velocity accuracy. Contours given for three levels of correlation.

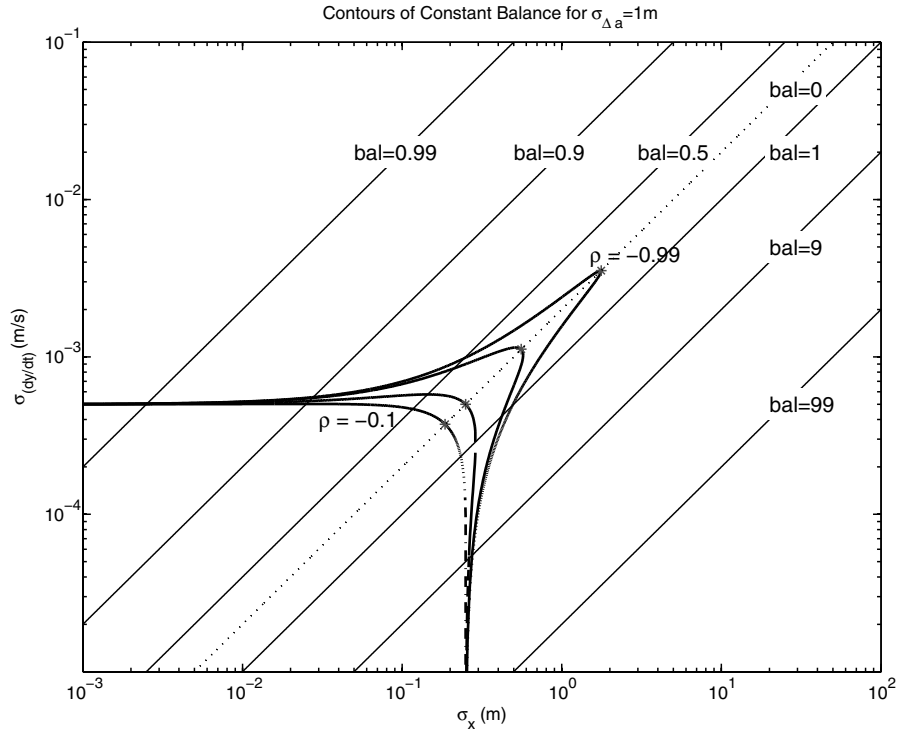

Fig. 2 Contours of constant balance (straight lines) illustrate regions where correlation affects SMA accuracy. Numbers indicate balance index and asterisks indicate points of perfect balance on the SMA contours.

approximation to perform a detailed analysis of the solution of a continuous Kalman filter, first for a system with position measurements and then for a system with position and velocity measurements. The following sections extend the numerical analysis to the more complicated case with a discrete Kalman filter.

Starting with the continuous Kalman filter using the in-plane components of Eq. (3)

$$\ddot{x} - 2n\dot{y} - 3n^2 x = f_x \tag{11}$$

$$\ddot{y} + 2n\dot{x} = f_y \tag{12}$$

where f_x and f_y are disturbance accelerations with identical spectral densities σ_Q^2. These equations of motion can be written in state space form using $X = [x, \dot{x}, y, \dot{y}]^T$ and dynamics matrices A_h and B_h. When only position measurements are available, the output matrix is

$$H_h = \begin{bmatrix} 1 & 0 & 0 & 0 \\ 0 & 0 & 1 & 0 \end{bmatrix} \tag{13}$$

with sensing noise given by σ_R^2 on each measurement. These dynamics can be transformed to a new system of equations with the state $\bar{X} = [x, x', y, y']^T$, where $(*)' = (\dot{*})\Delta t$, $\bar{X} = T_p X$, and

$$T_p = \text{diag}([\,1 \quad \Delta t \quad 1 \quad \Delta t\,])$$

to yield

$$x'' = 2\epsilon y' + 3\epsilon^2 x + (\Delta t)^2 f_x \tag{14}$$

$$y'' = -2\epsilon x' + (\Delta t)^2 f_y \tag{15}$$

with $\epsilon = n\Delta t$. Note that when $\epsilon \ll 1$, which is true for the cases of interest in this section, the x and y orbital dynamics can essentially be written as double integrators for which the solution of the Riccati equation is easily found. The combined dynamics then consist of these two double integrators with coupling terms of order ϵ and ϵ^2.

Remark 2: A Kalman filter, by definition, gives the minimum variance estimates of the relative states [13], which can then be used to produce the approximate minimum variance estimate of the semimajor axis difference. This follows because the relative semimajor axis is approximately a linear combination of radial position and in-track velocity, as shown in Eq. (5). The state vector could be transformed into a state that explicitly includes the semimajor axis:

$$\mathbf{x}_t = \begin{bmatrix} \Delta a \\ \dot{x} \\ y \\ \dot{y} \end{bmatrix} = \begin{bmatrix} 4 & 0 & 0 & 2/n \\ 0 & 1 & 0 & 0 \\ 0 & 0 & 1 & 0 \\ 0 & 0 & 0 & 1 \end{bmatrix} \begin{bmatrix} x \\ \dot{x} \\ y \\ \dot{y} \end{bmatrix} \equiv T\mathbf{x}$$

where T is the invertible transformation matrix between the nominal state and the transformed state. The Kalman filter objective function is related to the magnitude of the estimation error, which can be transformed as follows:

$$\tilde{\mathbf{x}}_t^T \tilde{\mathbf{x}}_t = (\hat{\mathbf{x}}_t - \mathbf{x}_t)^T(\hat{\mathbf{x}}_t - \mathbf{x}_t) = (\hat{\mathbf{x}} - \mathbf{x})^T T^T T(\hat{\mathbf{x}} - \mathbf{x}) = \tilde{\mathbf{x}}^T S \tilde{\mathbf{x}} \tag{16}$$

where $S = T^T T \geq 0$. From [13], the optimal estimate for the state $\mathbf{x}$ is found by minimizing the cost function:

$$J = E[\tilde{\mathbf{x}}^T M \tilde{\mathbf{x}}]$$

where M is any positive semidefinite matrix. The key point is that the optimal estimate is independent of the choice of $M \geq 0$ [13]. Because we can choose $M = I$, or $M = S$, as in Eq. (16), then the optimal estimate for $\mathbf{x}_t$ will be related to the optimal estimate for $\mathbf{x}_n$ by the linear transformation T. Thus, a Kalman filter estimating relative position and velocity *necessarily* will also yield the minimum variance estimate of the approximate relative semimajor axis, to within the error associated with the linearization. □

A. Correlation with Position Measurements

The dynamics in Eqs. (14) and (15) are written in state space form as

$$\bar{X}' = \bar{A}\bar{X} + \bar{B}f \tag{17}$$

where $\bar{A} = \Delta t(T_P A_h T_P^{-1})$, $\bar{B} = \Delta t(T_p B_h)$, and $\bar{H} = H_h$. The differential filter Riccati equation for the original system [Eqs. (11) and (12)] must also be transformed using T_p, and the result is that, at steady state

$$\mathbf{0} = \bar{A}P + P\bar{A}^T + \bar{B}Q\bar{B}^T - P\bar{H}^T R^{-1}\bar{H}P \tag{18}$$

where $Q = (\sigma_Q^2/\Delta t)I_2$ and $R = (\sigma_R^2/\Delta t)I_2$, with the factors of $1/\Delta t$ resulting from the transformation. To proceed, the covariance for the transformed state is represented as a Taylor expansion in ϵ. Substituting

$$P = P_0 + \epsilon P_1 + \epsilon^2 P_2 + \ldots \tag{19}$$

$$\bar{A} = A_0 + \epsilon A_1 + \epsilon^2 A_2 \ldots \tag{20}$$

in the Riccati equation and grouping terms in the same power of ϵ, it is possible to solve for the expansion of the covariance matrix ($P_{k_{xx}}$, $P_{k_{y'y'}}$, and $P_{k_{xy'}}$, $k = 0, 1, \ldots$). The $\bar{A}$ matrix in Eq. (17) gives the expansion matrices A_0 and A_1:

$$A_0 = \begin{bmatrix} A_{00} & 0_2 \\ 0_2 & A_{00} \end{bmatrix} \qquad A_1 = \begin{bmatrix} 0_2 & A_{11} \\ -A_{11} & 0_2 \end{bmatrix} \tag{21}$$

$$A_{00} = \begin{bmatrix} 0 & 1 \\ 0 & 0 \end{bmatrix} \qquad A_{11} = \begin{bmatrix} 0 & 0 \\ 0 & 2 \end{bmatrix} \tag{22}$$

Define the vectors

$$\boldsymbol{x} = [\,x \quad x'\,]^T$$

and

$$\boldsymbol{y} = [\,y \quad y'\,]^T$$

Then $P_{0\mathbf{xy}} = \mathbf{0}$ for the solution of the two independent double integrators. Using

$$A = \begin{bmatrix} 0 & 1 \\ 0 & 0 \end{bmatrix} \qquad B = \begin{bmatrix} 0 \\ \Delta t^2 \end{bmatrix} \qquad H = [\,1 \quad 0\,] \tag{23}$$

the first-order solution to the Riccati equation is

$$P_{0\mathbf{xx}} = P_{0\mathbf{yy}} = \begin{bmatrix} P_{0_{11}} & P_{0_{12}} \\ P_{0_{21}} & P_{0_{22}} \end{bmatrix} = \begin{bmatrix} \sqrt{2}\sigma_Q^{\frac{1}{2}}\sigma_R^{\frac{3}{2}} & \sigma_Q\sigma_R\Delta t \\ \sigma_Q\sigma_R\Delta t & \sqrt{2}\sigma_Q^{\frac{3}{2}}\sigma_R^{\frac{1}{2}}\Delta t^2 \end{bmatrix} \tag{24}$$

Substituting into the Riccati equation and isolating $\mathcal{O}(\epsilon)$ terms yields

$$P_0 A_1^T + P_1 A_0^T + A_0 P_1 + A_1 P_0 = P_0 D P_1 + P_1 D P_0 \tag{25}$$

$$P_1(A_0^T - DP_0) + (A_0 - P_0 D)P_1 = -(P_0 A_1^T + A_1 P_0) \tag{26}$$

where

$$D = \begin{bmatrix} C & 0_2 \\ 0_2 & C \end{bmatrix} \qquad C = \frac{\Delta t}{\sigma_R^2}\begin{bmatrix} 1 & 0 \\ 0 & 0 \end{bmatrix} \tag{27}$$

Using the knowledge that $P_{0\mathbf{xx}} = P_{0\mathbf{yy}}$,

$$\left(A_0^T - DP_0\right) = \begin{bmatrix} E & 0_2 \\ 0_2 & E \end{bmatrix} \tag{28}$$

where

$$E = \begin{bmatrix} -\frac{\Delta t P_{0_{\mathbf{xx}}}}{\sigma_R^2} & -\frac{\Delta t P_{0_{\mathbf{xx}'}}}{\sigma_R^2} \\ 1 & 0 \end{bmatrix} \tag{29}$$

and

$$(A_0 - P_0 D) = \begin{bmatrix} E^T & 0_2 \\ 0_2 & E^T \end{bmatrix} \tag{30}$$

Defining G as

$$G = A_{11}P_{0_{\mathbf{xx}}} - P_{0_{\mathbf{xx}}}A_{11}^T = \begin{bmatrix} 0_2 & -2P_{0\mathbf{xx}'} \\ 2P_{0\mathbf{xx}'} & 0_2 \end{bmatrix} \tag{31}$$

$$\left(P_0 A_1^T + A_1 P_0\right) = \begin{bmatrix} 0_2 & G \\ -G & 0_2 \end{bmatrix} \tag{32}$$

Substituting into the Riccati equation yields

$$\begin{bmatrix} P_{1_{\mathbf{xx}}} & P_{1_{\mathbf{xy}}} \\ P_{1_{\mathbf{xy}}^T} & P_{1_{\mathbf{yy}}} \end{bmatrix}\begin{bmatrix} E & 0_2 \\ 0_2 & E \end{bmatrix} + \begin{bmatrix} E^T & 0_2 \\ 0_2 & E^T \end{bmatrix}\begin{bmatrix} P_{1_{\mathbf{xx}}} & P_{1_{\mathbf{xy}}} \\ P_{1_{\mathbf{xy}}^T} & P_{1_{\mathbf{yy}}} \end{bmatrix} = -\begin{bmatrix} 0_2 & G \\ -G & 0_2 \end{bmatrix} \tag{33}$$

which is a system of three matrix equations

$$P_{1_{\mathbf{xx}}}E + E^T P_{1_{\mathbf{xx}}} = 0_4 \tag{34}$$

$$P_{1_{\mathbf{yy}}}E + E^T P_{1_{\mathbf{yy}}} = 0_4 \tag{35}$$

$$P_{1_{\mathbf{xy}}}E + E^T P_{1_{\mathbf{xy}}} = -G \tag{36}$$

The solution to Eqs. (34) and (35) is $P_{1\mathbf{xx}} = P_{1\mathbf{yy}} = 0$, and Eq. (36) gives

$$P_{1_{xy'}} = -\frac{2\sigma_R^2 P_{0_{xx'}}}{\Delta t P_{0_{xx}}} \qquad P_{1_{x'y}} = -P_{1_{xy'}} \qquad P_{1_{x'y'}} = P_{1_{xy}} = 0 \tag{37}$$

Then the correlation coefficient can be found from

$$\rho_{x\dot{y}} = \frac{P_{x\dot{y}}}{\sqrt{P_{xx}P_{\dot{y}\dot{y}}}} = \frac{P_{xy'}/\Delta t}{\sqrt{P_{xx}P_{y'y'}/\Delta t^2}} \approx \frac{\epsilon P_{1xy'}}{\sqrt{P_{0xx}P_{0y'y'}}} \tag{38}$$

Using the expressions previously given, it follows that

$$\rho_{x\dot{y}} \approx -\frac{2(n\Delta t)\sigma_R^2(\sigma_Q\sigma_R\Delta t)}{\sqrt{2}\Delta t\sigma_Q^{1/2}\sigma_R^{3/2}}\left(\sqrt{2}\sigma_Q^{1/2}\sigma_R^{3/2}\sqrt{2}\sigma_Q^{3/2}\sigma_R^{1/2}\Delta t^2\right)^{-1/2} = -\frac{\sqrt{2}n\sigma_R^{3-(3/2)}\sigma_Q^{1-(1/2)}\Delta t}{\sqrt{2\sigma_Q^2\sigma_R^2\Delta t^2}} \tag{39}$$

$$\approx -n\sqrt{\frac{\sigma_R}{\sigma_Q}} \tag{40}$$

which, upon substitution in Eq. (7), gives a semimajor axis error of

$$\sigma_{\Delta a} \approx (2^{5/4}/n)\sigma_Q^{3/4}\sigma_R^{1/4} \tag{41}$$

Finally, applying the state transformation T_p to $P_{0\mathbf{yy}}$ in Eq. (24), it follows that, because

$$\sigma_{\dot{y}} \approx \left(2^{1/2}\sigma_Q^{3/2}\sigma_R^{1/2}\right)^{1/2}$$

then the semimajor axis error can be rewritten as

$$\sigma_{\Delta a} \approx (2/n)\sigma_{\dot{y}} \tag{42}$$

Note that in Eq. (42) the resulting semimajor axis variance is only a function of the in-track velocity variance, even though the semimajor axis error is a function of the radial position and in-track velocity errors. This occurs because the radial position variance and correlation terms are equal and of opposite sign, and so they cancel each other.

Equations (40) and (42) are the predictions of the correlation and semimajor axis variances from a perturbation analysis of a continuous Kalman filter that has two decoupled double integrators as the first approximation. Therefore, some discussion of the effect of these approximations on the validity range of the answers is in order. However, as will be seen, these equations agree well with the simulation results shown in later sections. The small parameter in the perturbation analysis is $\epsilon = n\Delta t$, therefore, as $\epsilon \to \mathcal{O}(1)$, they will no longer be valid. For low Earth orbits $n \approx 0.001$, consequently, when $\Delta t > 100$ s, the approximation should be expected to start degrading and when $\Delta t \approx 1000$ s it would not be expected to be valid. In addition, by definition $|\rho_{x\dot{y}}| \leq 1$, which gives that

$$\sigma_Q/\sigma_R \geq n^2 \tag{43}$$

Because $n \approx 0.001$, this implies that σ_R should be no more than six orders of magnitude larger than σ_Q. For example, consider that many space-rated GPS receivers produce differential carrier-phase measurements with millimeters of error. Equation (43) indicates that to achieve $\rho_{x\dot{y}} = -1$, the dynamics environment of the vehicle would have to be modeled to nanometer-level accuracy, which is currently not possible. For a typical scenario [11], $\sigma_Q = 1 \times 10^{-6}$ m/s$^{3/2}$ and $\sigma_R = 5 \times 10^{-3}$ m/s$^{1/2}$, which gives that

$$|\rho_{x\dot{y}}| \approx 1 \times 10^{-3}\sqrt{\frac{5 \times 10^{-3}}{1 \times 10^{-6}}} = 0.0707 \ll 1$$

which is consistent with the low levels of correlation found in current CDGPS results.

B. Examination of Balance Requirement

One strategy for minimizing the semimajor axis error is to achieve a high correlation and to simultaneously have a balance of errors given by

$$\sigma_{\dot{y}}/\sigma_x = 2n \tag{44}$$

For the transformed state described by Eqs. (14) and (15), this requirement is

$$\sigma_{y'}/\sigma_x = 2n\Delta t \tag{45}$$

Equation (24) showed that for the HCW equations, to first order, the standard deviations for in-track velocity and radial position estimates are

$$\sigma_{y'} \approx \sqrt{P_{0_{y'y'}}} = \left(\sqrt{2}\sigma_Q^{3/2}\sigma_R^{1/2}\Delta t^2\right)^{1/2} \tag{46}$$

$$\sigma_x = \sqrt{P_{\mathbf{xx}}} \approx \sqrt{P_{0_{\mathbf{xx}}}} = \left(\sqrt{2}\sigma_Q^{1/2}\sigma_R^{3/2}\right)^{1/2} \tag{47}$$

Substituting into Eq. (44) gives the analytic expression for the balance condition

$$\sigma_{y'}/\sigma_x = \sqrt{\frac{\sqrt{2}\sigma_Q^{3/2}\sigma_R^{1/2}\Delta t^2}{\sqrt{2}\sigma_Q^{1/2}\sigma_R^{3/2}}} = \Delta t\sqrt{\frac{\sigma_Q}{\sigma_R}} \tag{48}$$

Using Eq. (44), perfect balance requires that

$$\Delta t\sqrt{\sigma_Q/\sigma_R} = 2n\Delta t \Rightarrow \sqrt{\sigma_R/\sigma_Q} = 1/2n \tag{49}$$

This expression can be substituted into Eq. (40) to find the correlation that is achieved when the balance is correct

$$\rho_{x\dot{y}} = -n\sqrt{\sigma_R/\sigma_Q} = -n\Big(1/2n\Big) = -0.5 \tag{50}$$

This analysis shows that, for the Kalman filter, achieving the required balance is incompatible with achieving a correlation of -1.

C. Correlation with Position and Velocity Measurements

In this example, the system is augmented with a velocity sensor to investigate if direct velocity measurements can be used to achieve the correlation and balance requirements. The sensor noise and measurement matrices for the transformed double integrator dynamics now take the form

$$R = \frac{1}{\Delta t}\begin{bmatrix} \sigma_{rx}^2 & 0 \\ 0 & \sigma_{r\dot{x}}^2 \end{bmatrix} \qquad H = \begin{bmatrix} 1 & 0 \\ 0 & \Delta t^{-1} \end{bmatrix} \tag{51}$$

and the process noise term remains $Q = (\sigma_Q^2/\Delta t)I_2$. Substituting into the Riccati equation and solving for the terms in the first-order covariance matrix yields

$$P_{0_{11}} = \sqrt{2}\sigma_{rx}^{3/2}\sigma_Q^{1/2}\left[\frac{(1+0.5K)^{1/2}}{(1+K)}\right]$$

$$P_{0_{22}} = \sqrt{2}\sigma_{rx}^{1/2}\sigma_Q^{3/2}\Delta t^2\left[\frac{(1+0.5K)^{1/2}}{(1+K)}\right] \qquad P_{0_{12}} = \frac{\sigma_{rx}\sigma_Q\Delta t}{(1+K)} \tag{52}$$

where $K = \sigma_Q\sigma_{rx}/\sigma_{r\dot{x}}^2$. Substituting Eq. (52) into the HCW expansion in Eq. (26) yields a matrix equation in the same form as Eq. (33), however, the matrix D is now redefined as

$$D = \begin{bmatrix} \bar{C} & 0_2 \\ 0_2 & \bar{C} \end{bmatrix} \qquad \bar{C} = \begin{bmatrix} \Delta t/\sigma_{rx}^2 & 0 \\ 0 & 1/(\sigma_{r\dot{x}}^2\Delta t) \end{bmatrix} \tag{53}$$

This set of matrix equations also indicates that $P_{1_{\mathbf{xx}}} = P_{1_{\mathbf{yy}}} = 0_2$. The remaining solution is of the form

$$P_{1_{xy}} = P_{1_{x'y'}} = 0_2 \tag{54}$$

$$P_{1_{xy'}} = -P_{1_{x'y}} = -2\frac{\sigma_{rx}^2 P_{0_{xx'}}}{\Delta t P_{0_{xx}}}\left(\frac{1}{1+K}\right) \tag{55}$$

Solving for the correlation coefficient $\rho_{x\dot{y}}$ gives

$$\rho_{x\dot{y}} \approx \frac{\epsilon P_{1_{xy'}}}{(P_{0_{xx}}P_{0_{y'y'}})^{\frac{1}{2}}} \approx -n\sqrt{\frac{\sigma_{rx}}{\sigma_Q}}\left(\frac{1}{1+0.5K}\right) \tag{56}$$

From Eq. (56), it can be seen that as the velocity measurement becomes more accurate (K increases), the correlation magnitude is reduced. This is consistent with the observation that the filter makes more use of dynamics when there are fewer measurements. Substituting this value for $\rho_{x\dot{y}}$ into the expression for semimajor axis standard deviation yields

$$\sigma_{\Delta a} = \frac{2^{5/4}}{n}\sigma_{rx}^{1/4}\sigma_Q^{3/4}\left[\frac{\sigma_Q\sigma_{rx} + 4\sigma_{rx}^2n^2 + 2\sigma_{r\dot{x}}^2}{\sigma_Q\sigma_{rx} + \sigma_{rx}^2n^2 + 2\sigma_{r\dot{x}}^2}\right]^{1/2} \times \left[\frac{(1+0.5K)^{1/4}}{(1+K)^{1/2}}\right]\left[1 + 0.5\left(\frac{n\sigma_{rx}}{\sigma_{r\dot{x}}}\right)^2\frac{1}{1+0.5K}\right]^{1/2} \tag{57}$$

where the new semimajor axis standard deviation is no longer solely a function of the velocity accuracy. Equation (57) predicts that SMA knowledge can be improved by reductions in process noise and improvements in position and velocity sensing accuracy.

IV. Analysis on a Linear Planar Model

A Kalman filter produces the minimum variance estimate of the approximate relative semimajor axis, but does not necessarily meet the balance and correlation requirements. Numerical simulations in this section show the filter cannot be forced to meet both the balance and correlation requirements by adjusting the input parameters, supporting the analytical conclusions of the previous section. There are many parameters that must be specified for a Kalman filter and all of these affect the accuracy of the estimates. The dynamics and measurement models, the operating environment, and the extent to which nonlinearities are accentuated may all affect the process Q and sensor R noise intensities. The set of sensor data made available to the filter will determine the measurement matrix H. Also, the time step can affect the performance of the discrete filter. The relationship between design parameters and navigation accuracy is investigated and this should lead to a better understanding of what changes might be required to improve navigation.

A CDGPS navigation filter has nonlinearities in both the system dynamics and the measurement equations, and because the set of visible GPS satellites changes, the measurement matrix H and the geometric dilution of precision (GDOP) will change, and the state vector length will grow or shrink as the set of estimated carrier biases changes [12]. These factors make it difficult to understand direct relationships between the filter parameters and the navigational accuracies. Thus, the following starts with a simplified linear planar model (LPM) to develop insights into the behavior of a relative navigation filter using CDGPS. Table 1 summarizes the Kalman filter parameters considered in the LPM simulations.

Table 1 Kalman filter elements for LPM simulations

Description	Notation	Simulation
Dynamics model	A	Planar HCW equations, constant in simulations
Measurements model	H	Direct measures of position; GDOP varied by changing number and direction of measurements
Discrete time step	Δt	Varied
Process noise	Q	Varied, to highlight effects of mismodeled dynamics
Measurement noise	R	Varied, to change quality of measurements

The system dynamics in the LPM are taken from the solutions of the HCW equations for radial and in-track position and velocity. Out-of-plane motion is ignored, because it does not affect semimajor axis error. The dynamics model is not varied in the simulations, but its effective accuracy is modified by evaluating filter performance with different values of Q. Most state-of-the-art GPS receivers can provide as many as 12 pseudorange measurements. Similarly, the LPM includes two or more direct measures of position that span the orbital plane. Variations of the measurement model included changing the angle between two position measurements and increasing the number of measurements included. Also, the level of noise associated with the measurements is varied. Different discrete time steps Δt are considered in these simulations. Note that as the time step changes, the relative importance of the dynamics model and the measurements will change. For example, if highly accurate measurements are provided at a very fast rate, the dynamics model might be of little importance. Conversely, once the estimate has converged, a perfect propagator might not need any future measurements. Changing the time step should illuminate how the filter might favor one of these extremes.

The simplified LPM problem will show how each parameter affects the radial position error and in-track velocity error, the correlation of the two, and, ultimately, the semimajor axis error. For each design variation, the position and velocity variances are found by numerically solving a discrete algebraic Riccati equation. The position and velocity error variances from Eq. (18) are used in Eq. (7) to compute the corresponding semimajor axis error.

A. Two LPM Examples for Correlation Demonstrations

Because the measurements span the orbital plane, it is intuitive that the correlation between radial position and in-track velocity will increase only when the estimate depends more on the dynamics model embedded in the filter. The following examples (see results in Figs 3–6) induce this behavior:

1) The angle between the two measurements is increased from 0 to 90 deg, as in Fig. 3. This causes the direct observability of the orbital plane to decrease as the two measurements become aligned and results in the term $H^TR^{-1}H$ in the Kalman filter losing full rank. Because the measurements no longer span the full orbital plane, the dynamics model must be employed to create estimates of all x and y states.

2) The number of measurements is reduced from six to one, causing changes in the direct observability.

The results from these examples are discussed next.

Example 1: This example provides an excellent view of how the span of the measurement matrix affects the correlation and semimajor axis error. The two position measurements have equal accuracy and are initially aligned with the x and y axes. The angle between the two measurements is gradually decreased until the

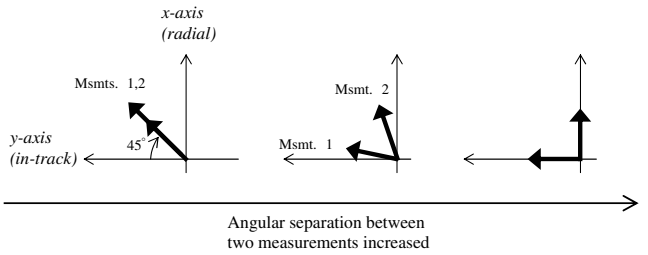

Fig. 3 LPM Example 1: filter performance as two measurements are brought into alignment.

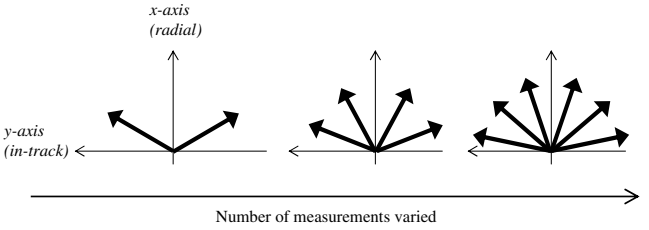

Fig. 4 LPM Example 2: filter performance as the number of measurements is varied.

measurement directions are nearly colinear at a 45-deg angle in the x–y plane. Figure 5 shows that the correlation between the two remains low until the angular separation is less than ∼20 deg. When the angular separation becomes smaller than a degree, the correlation drops sharply from −0.7 toward −1. Clearly, as the measurements approach alignment, the uniqueness of the information that each contributes decreases, and the results show that the correlation rapidly approaches −1 as the system dynamics become more important. However, when the measurements no longer span the orbital plane, the results also show that the position and velocity errors increase dramatically. Because the balance requirement is not met exactly, the increased errors in position and velocity outweigh the advantage of the increased correlation, and the final semimajor axis error is large. In the example shown, the two measurement directions converged on 45 deg, but similar results were seen for other terminal angles.

Example 2: This example, seen in Fig. 4, looks at the effect of changing the number of measurements, which are equally spaced in the orbital plane. When a second measurement is added, the values of σ_x and $\sigma_{\dot{y}}$ drop sharply (see Fig. 6), $\rho_{x\dot{y}}$ changes from close to −1 to approximately −0.5, and the balance index increases. The state estimates are further from meeting the correlation and balance requirements, but the semimajor axis knowledge improves. In cases where correlation and balance conditions cannot be met simultaneously, the goal for achieving low semimajor axis error can still be achieved by minimizing estimation errors. The results of this example also show that, as further measurements are added, the position, velocity, and semimajor axis errors all improve, although the correlation decreases. This is consistent with behavior seen in the first example.

Remark 3: In these examples, the filter can be forced to rely on its dynamics model to extract good state information in the radial and in-track directions. This increased reliance is accomplished by degrading the available sensing information. The increases in σ_x and $\sigma_{\dot{y}}$ that accompany the higher correlation consistently result in a larger semimajor axis error. This is a trait of a filter that is measurement-dependent, not a symptom of deficiency. When the correlation between radial position and in-track velocity is low, the best strategy for determining relative semimajor axis is to estimate both quantities with the highest possible accuracy, and the Kalman filter does exactly that. The behavior seen in both variations of this simplified example provide insight into the relative navigation system using CDGPS measurements. A GPS-based navigation filter will typically have many position-related measurements available (9–12). The estimator can be forced to have better correlations by degrading the measurements and boosting the importance of the dynamics model. However, these examples show that this would result in increased semimajor axis error and is a suboptimal strategy. □

B. LPM Simulations with Q and R

This section investigates the relationship between the Kalman filter parameters and the resulting estimate accuracy. The levels of measurement and process noise are indicators of how well the sensors and the dynamics are modeled, and their relative values determine how the filter weighs new measurement information against the current state estimate propagated using the dynamics.

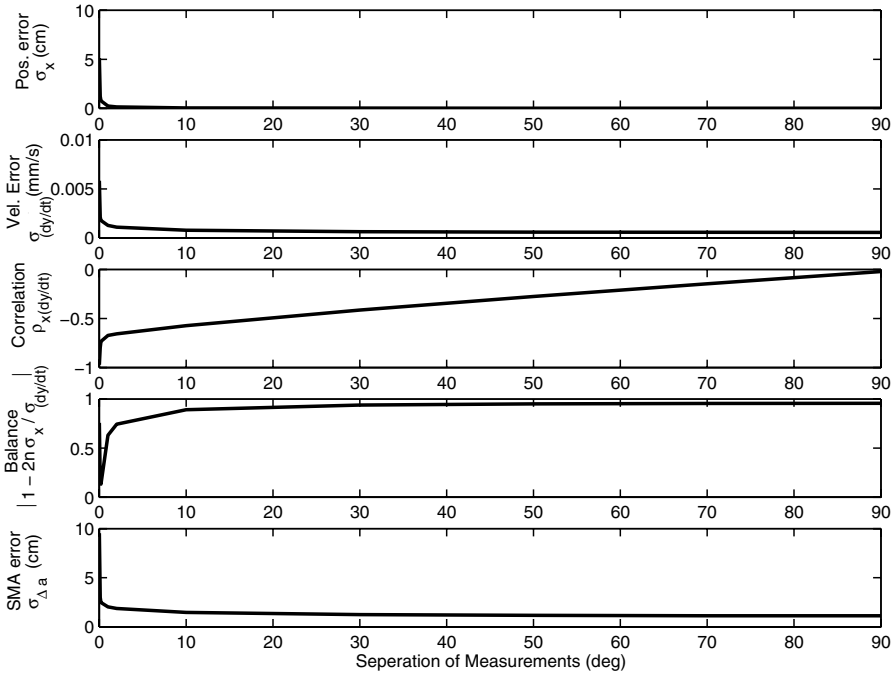

Fig. 5 LPM Example 1: filter performance vs angular separation; $\Delta t = 1$ s.

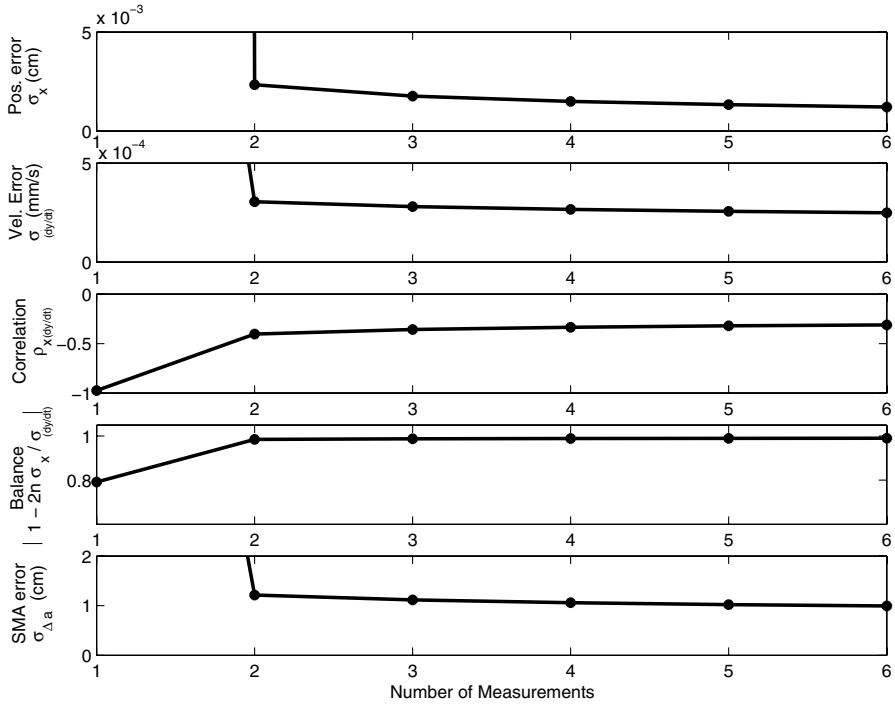

Fig. 6 LPM Example 2: filter performance vs number of measurements.

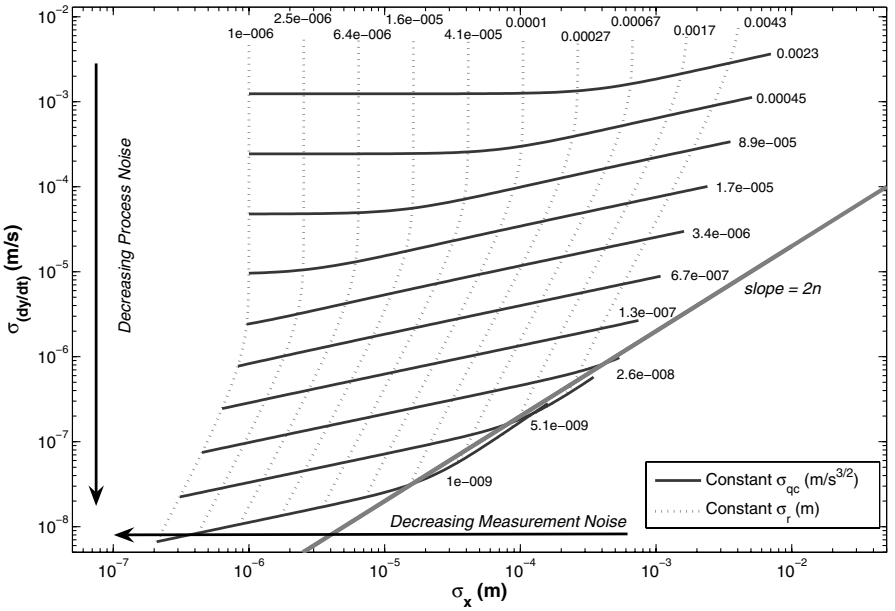

Fig. 7 Contours of constant Q and R, shown on axes of position and velocity accuracy.

Meeting the balance and correlation requirements discussed in Sec. I corresponds to being on the bump in Fig. 1. The LPM results shown here occupy the region above the $\sigma_{\dot{y}} = 2n\sigma_x$ line, which occurs because the balance requirement is not met and is dominated by the velocity errors for this position-measurement-based CDGPS system. This leads to the question of how changing filter inputs will move the output closer to or further from the bump. To answer this question, the LPM simulation was run for a range of measurement and process noise levels. For each unique assignment of Q and R, the resulting error variances for radial position and in-track velocity, σ_x and $\sigma_{\dot{y}}$, were recorded. The corresponding semimajor axis error $\sigma_{\Delta a}$ was calculated using Eq. (7). Fig. 7 shows lines of constant Q and R on axes of σ_x and $\sigma_{\dot{y}}$, where $Q = \mathrm{diag}(0_2, \sigma_{qc}^2 I_2)$, $R = \sigma_r^2 I_2$, σ_{qc} is the continuous process noise covariance, and σ_r is the discrete measurement covariance. The diagonal of peaks on this graph indicates the location of the bump, where the balance and correlation requirements are met (which means $\sigma_{\dot{y}} = 2n\sigma_x$). By moving from one line of constant Q or R to another, one can see how decreasing the process or measurement noise would change the resulting position and velocity error.

Several graphs are presented to demonstrate the relationship between Q, R, and $\sigma_{\Delta a}$. First, Fig. 8 reproduces Fig. 7 and lines of constant semimajor axis error are added. The lines for constant Q and R are dimmed for clarity. Note the lines of constant semimajor axis are horizontal, which corresponds with the horizontal sections of the semimajor axis contours on Fig. 1. The effect of changes in Q and R on $\sigma_{\Delta a}$ can be assessed by looking at the constant lines for all three values. Because the lines of constant semimajor axis are horizontal, improvement in $\sigma_{\Delta a}$ can only be accomplished by moving in the vertical direction on the graph, which is equivalent to decreasing $\sigma_{\dot{y}}$.

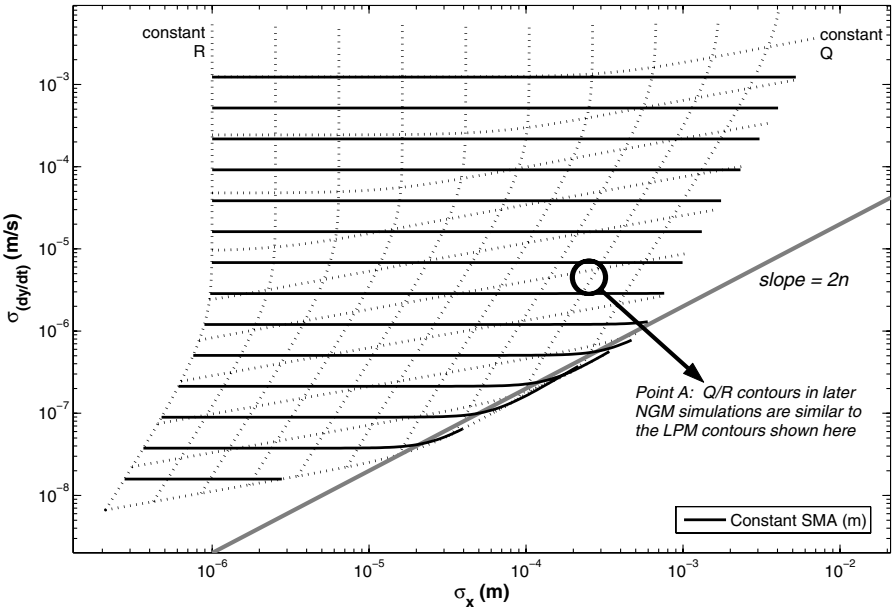

Fig. 8 Contours of constant semimajor axis shown vs position/velocity accuracy. Contours of constant Q and R are background dotted lines.

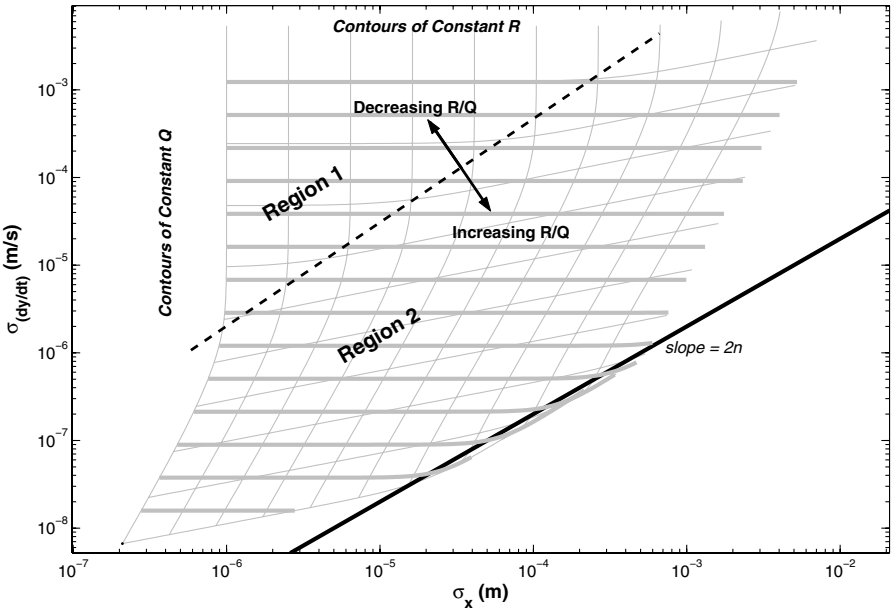

Fig. 9 In region 1, decreasing the semimajor axis error requires decreasing the process noise level. In region 2, decreasing either process or measurement noise can reduce semimajor axis error.

Whether this requires decreasing Q or R depends on the angles between the horizontal lines of constant $\sigma_{\Delta a}$ and the contours of constant Q and R.

Two regions are indicated in Fig. 9. Region 1 (upper left hand portion of the graph) contains lines of constant Q and R that are essentially horizontal and vertical, respectively. Improving the measurement noise in this region (or, essentially, moving horizontally in the graph) has minimal effect on semimajor axis knowledge. Decreasing $\sigma_{\Delta a}$ would require improving the process noise to enable vertical movement on the graph. Region 2 is closer to the line of $\sigma_{\dot{y}} = 2n\sigma_x$. Here, the lines of constant Q and R are no longer parallel and perpendicular to the horizontal lines of constant semimajor axis. This means that reducing either Q or R could improve $\sigma_{\Delta a}$. This shift from region 1, where sensing improvement has virtually no effect on $\sigma_{\Delta a}$, to region 2, where it does, is also shown in Fig. 10 by plotting contours of constant semimajor axis on axes of Q and R. As expected, region 1 has horizontal lines of constant $\sigma_{\Delta a}$, which directly shows that decreasing the measurement noise has little effect on semimajor axis knowledge. The portion of the graph where the contours of constant $\sigma_{\Delta a}$ are sloped corresponds to region 2. In this region, improvements in the measurements or the dynamics models (i.e., reduced process noise) would contribute to improved semimajor axis knowledge.

C. Discrete Simulations for Varying Δt

One additional way to put more emphasis on the dynamics model is to reduce the measurement rate. Prior analysis of the CDGPS filter by Busse [12] used a 1 Hz rate, although much longer time steps were considered in [11]. One difficulty with increasing the propagation time is that the nonlinearity in the orbit propagation becomes much more significant and more sophisticated models and propagation algorithms must be used, especially for the error covariance [14,15]. The following investigation of the effect of varying measurement update rate by changing the discretization time step uses the linear model and thus ignores these effects.

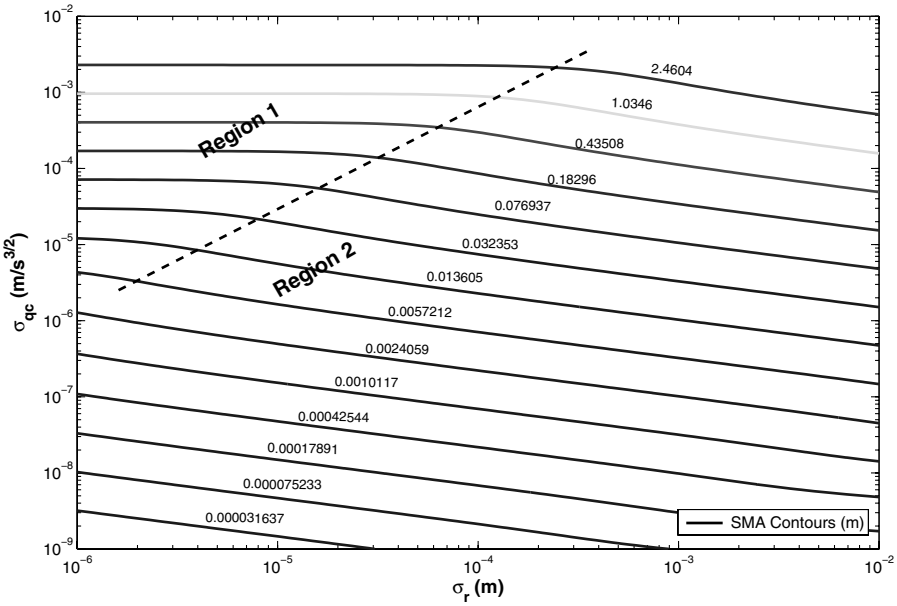

Fig. 10 Contours of constant semimajor axis shown against Q and R. In region 1, process noise alone impacts semimajor axis error, but in region 2, both noise levels impact this error.

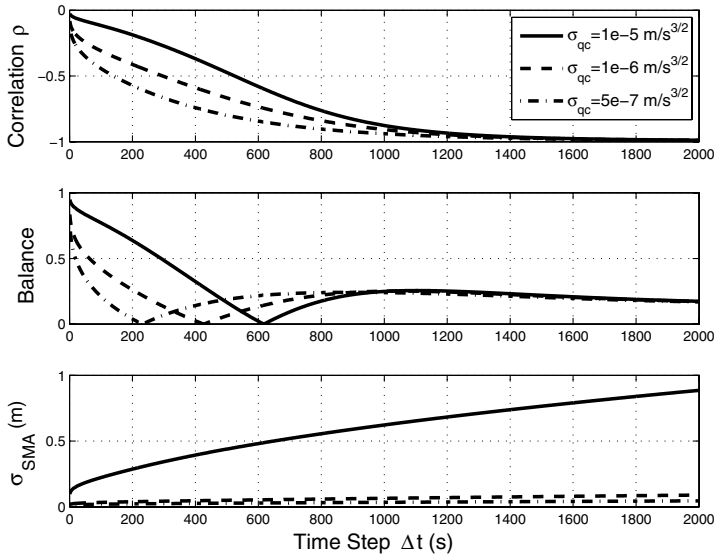

Fig. 11 Filter correlation, balance, and SMA error for various discretization time steps Δt (seconds).

To do this, a family of discrete Riccati equations was solved using HCW dynamics at various discretization times. In each case, the constant spectral density matrix Q_c associated with the process noise of the continuous dynamics was converted to the appropriate discrete process noise Q_d using the conversion algorithm in [16] (DISRW in Chapter 9). The simulation results in Fig. 11 were done for several values of $\sigma_{qc} = \{10^{-5}, 10^{-6}, 5 \times 10^{-7}\}$ m/s$^{3/2}$ ($Q_c = \sigma_{\text{qc}}^2 I_2$) and a constant sensing noise covariance $R = (5 \times 10^{-3}\ \text{m})^2$. The plot shows that, as the discretization time step is increased, the correlation coefficient tends to -1. This trend is expected, because longer propagation times will force increased filter dependence on the equations of motion, translating into increased overall correlation. However, the proper position to velocity error balance is not achieved, causing the SMA accuracy to degrade. The plot clearly shows the role of the process noise Q_c in determining the SMA error growth. One caveat about these results is that the correlation approaches -1 for filter time steps larger than 1000 s, for which the nonlinearity in the system dynamics, that this analysis ignores, may begin to play an important role [11].

Comparing this result with Fig. 2, it can be seen that although the balance index is not zero, it is producing the effect of lowering the overall semimajor axis in combination with the correlation. However, the canceling effects of correlation and balance are not sufficient to prevent the semimajor axis error from growing rapidly as the time step is increased. Thus, decreasing the measurement update rate to produce higher correlation is not a viable strategy for reducing semimajor axis error.

These examples considered the navigation filter accuracy for a linear planar model, and the next section explores similar questions using a full nonlinear GPS model (NGM).

V. Nonlinear GPS Model

The LPM simulations provide a base for discussion of the relationship between noise and filter performance in the full nonlinear GPS model. The NGM adds the clock and bias terms to the filter state definition and introduces uncertainties associated with the clock, ionosphere, absolute state error, etc. A similar exploration of the relationship between Q, R, and $\sigma_{\Delta a}$ is undertaken.

Two sets of NGM simulations, discussed next, will illustrate the relationship between process and measurement noises and estimator performance. The NGM analysis begins with a very simple model

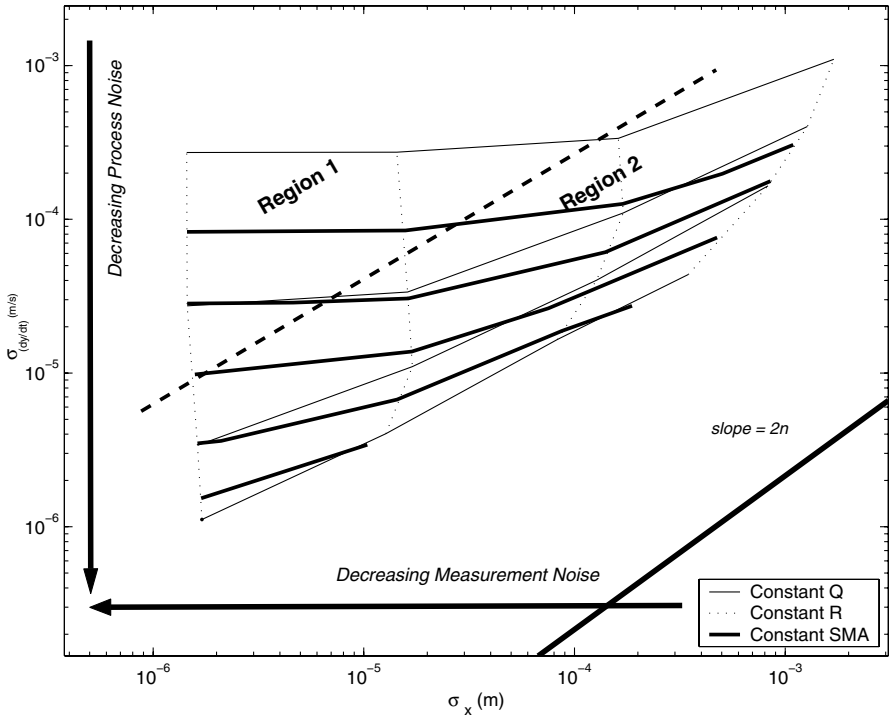

Fig. 12 Contours of constant Q and R and semimajor axis for NGM results. Nonlinear effects were minimized for this simulation, which was run with a 0.1 s time step.

that focuses on the relative orbital dynamics and GPS measurements and takes steps to reduce nonlinearities associated with their equations. The second set of simulations incorporates elements that more closely resemble a real-world scenario.

The NGM simulation environment is an extension of tools developed by Busse [11]. The user can specify which nonlinear effects and perturbations are included in the truth model and how they are accounted for in the filter, which is useful when comparing the NGM and the LPM results. The NGM simulation propagates all relevant vehicle truth states and provides simulated measurements to the estimator. Because a large number of simulations were required to observe relationships between filter parameters and the navigation accuracy, it was not practical to employ hardware-in-the-loop simulations that could provide the filter with actual measurements. The absolute truth states for the vehicles were used to create the simulated GPS measurements. The relative truth states were created by differencing the absolute states.

As in the LPM experiments, for each set of simulations, the NGM was run for an array of values of Q and R. Each full GPS simulation was run for 3000 s, to allow sufficient time for the filter to converge to steady state. The position and velocity errors were determined from the standard deviation of the estimation error, not from a Riccati equation as in the LPM cases. Note that in the nonlinear case, Eq. (7) was found to give inaccurate estimates of the semimajor axis error, and so orbital elements calculations were required. The absolute semimajor axes were differenced at each time step and used to find the estimation error for the differential semimajor axis. The square root of the variance of the steady-state estimation errors was recorded.

The goal of the first simulation set is to uncover the basic relationships between process and measurement noises and the semimajor axis error. These first simulations use the full NGM state, with clock and carrier bias terms included, and incorporates simulated GPS measurements. However, to maintain LPM-like simplicity, many real-world effects, such as ephemeris error, clock error, communication outages, and measurement cycle slips, are not included. Truncation error is reduced by placing the vehicles 1 m apart, and running the filter at a 0.1 s time step. The small separation distance also ensures the line-of-sight vectors to the GPS satellites for the two vehicles to be nearly identical (another assumption in the filter design).

The results of the first simulation set are shown in Fig. 12. The contours of constant Q, R, and $\sigma_{\Delta a}$ are very similar to those seen using the LPM. As in the LPM, region 1 contains lines of constant Q and R that are essentially horizontal and vertical. Improving the measurement noise in this region would have no effect on semimajor axis knowledge. Reductions in process noise are required to reduce $\sigma_{\Delta a}$. In region 2, improvements in the measurements or the process noise would contribute to improved semimajor axis knowledge. These observations confirm that the results of a simplified version of the NGM approach those of the LPM.

The second set of NGM simulations incorporates all available error sources in the models for the environment and sensors, including errors introduced by clock, ephemeris, and absolute state uncertainty. This setup is more representative of a real-world CDGPS filter in the LEO environment. The results of this set of simulations are shown in Fig. 13, with lines of constant Q, R, and $\sigma_{\Delta a}$ on the axes of σ_x and $\sigma_{\dot{y}}$. The line of $\sigma_{\dot{y}} = 2n\sigma_x$ is included as a reference, but will not necessarily represent the same transition point that it did in the LPM. The region that coincides with typical CDGPS accuracy is indicated on the plot.

Contours of constant process noise tend to the horizontal direction and contours of constant measurement noise tend towards vertical. The parallelograms formed by the contours of constant Q and R are indicative of general agreement between the LPM and NGM results (see point A in Figs. 8 and 13). However, going from the LPM to the NGM, the horizontal lines of constant semimajor axis become positively sloped. This indicates that in the NGM, position accuracy will have some effect on $\sigma_{\Delta a}$, where in the LPM, it had no effect. The slope of the NGM contours is still small, suggesting the velocity error still dominates semimajor axis knowledge.

This leads to a key observation about the performance of our CDGPS-based relative navigation filter. Reducing either process or measurement noise can have a positive effect on semimajor axis knowledge. Previous work assumed that a coarse dynamics model would be sufficient, because the measurement updates are performed very frequently and, based on that premise, a very accurate filter was developed [11]. However, this NGM analysis suggests future work that incorporates a higher-fidelity dynamics model, thereby

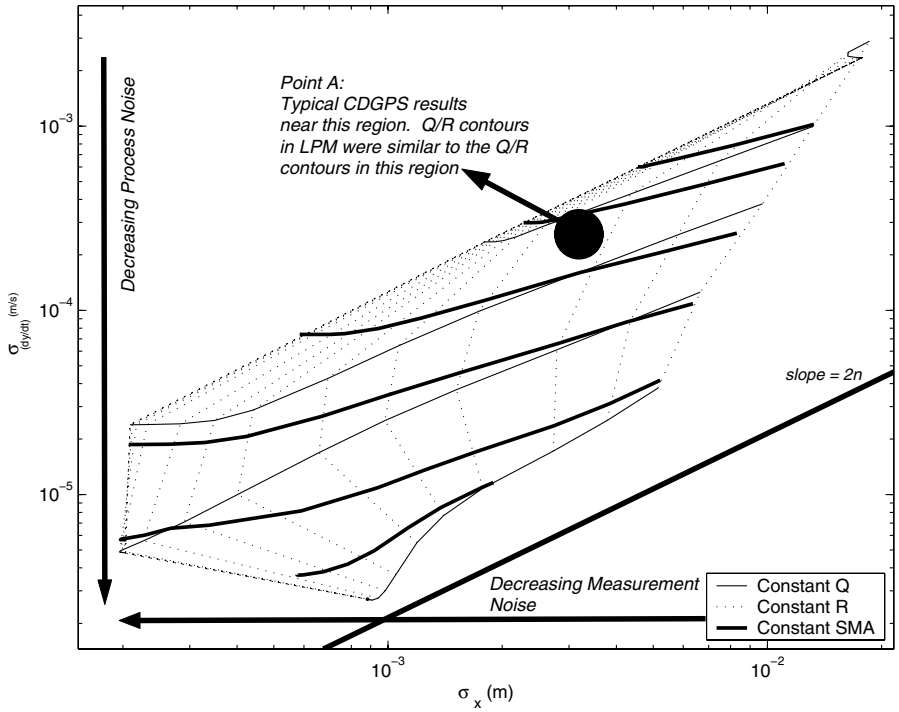

Fig. 13 Contours of constant Q and R and semimajor axis are shown for NGM results. This NGM included clock, ionospheric, and absolute state errors.

reducing the process noise, could improve the semimajor axis knowledge.

A departure from LPM behavior is seen in the lines of constant measurement noise. In the LPM case, reducing measurement noise always resulted in reductions of σ_x. In region 1 of the LPM (Fig. 9) the lines of constant R are vertical and orthogonal to the lines of constant semimajor axis. In other words, by increasing the sensor accuracy, it was always possible to keep improving σ_x. At some point, though, increasing sensor accuracy stopped improving semimajor axis knowledge. However, in the NGM cases, the contours of constant R bunch together as the sensor noise becomes very small, which implies that further reductions will not impact either $\sigma_{\Delta a}$ or σ_x. The fact that σ_x does not continue to improve as the measurement noise is decreased suggests that aspects of the NGM that reflect realistic phenomenon, such as clock error, become dominant. This leads to the second observation that noise sources other than the CDGPS measurements and the relative orbital dynamics model, such as from the clock and absolute state error, can limit the relative navigation filter performance. When these real-world errors are introduced in the NGM, there is a limit to how much the position, velocity, and semimajor axis performance can be improved. In contrast to the LPM, increasing sensor accuracy will not always result in similar increased position accuracy in the NGM.

Although some differences appear to be due to the nonlinearities in the NGM, the general trends, especially in the regions of the plots where typical CDGPS filter results are found, are retained. The similarities between the linear and nonlinear results suggest the observations from LPM-based filter behavior extend to filters based on the nonlinear dynamics and measurements. In particular, the insights gained from the LPM examples about the relationships between correlation, balance, and navigation errors, and between the process/measurement noises and the semimajor axis errors, are relevant to the more complex CDGPS filters.

VI. Conclusions

This paper was motivated by the desire to determine what metrics should be used to characterize the performance of a carrier-phase differential Global Positioning System relative navigation filter as "good," and explore what parameters in the Kalman filter have the most impact on the performance of the navigation system. Previous works had suggested that a good navigation filter would yield estimates of the along-track velocity and radial position that satisfy both the correlation and balance requirements. This paper presented detailed analysis and numerical simulations to show that the optimal approximate relative semimajor axis estimate from a Kalman filter does not satisfy these properties, for any combination of measurement and process noise, which is consistent with recent practical experience with CDGPS filters, even when the state estimates are very accurate. These results also highlighted the importance of developing good models of the process noise to improve the semimajor axis estimation performance.

Acknowledgment

This work was funded under Cooperative Agreements NCC5-729 and NCC5-724 through the NASA GSFC Formation Flying NASA Research Announcement.

References

[1] Williamson, J. B., "An Empirical Technique for Computing Navigation Covariance Matrices and the Application of the Technique to Post Apollo 8 Lunar Orbit Mission Planning," NASA Manned Spacecraft Center, Internal Note 69-FM-149, June 2, 1969.

[2] Lear, W. M., "Orbital elements including the J2 harmonic," NASA Johnson Space Center, Internal Note 86-FM-18/JSC-22213, Rev. 1, 1968.

[3] Carpenter, J. R., and Schiesser, E., "Semimajor Axis Knowledge and GPS Orbit Determination," *Journal of the Institute of Navigation*, Vol. 48, No. 1, 2001, pp. 1–20.

[4] Carpenter, J. R., and Alfriend, K. T., "Navigation Accuracy Guidelines for Orbital Formation Flying," *AIAA Guidance, Navigation, and Control Conference*, AIAA, Reston, VA, 2003, pp. 1–7.

[5] How, J. P., and Tillerson, M., "Analysis of the Impact of Sensor Noise on Formation Flying Control," *Proceedings of the American Control Conference*, Institute of Electrical and Electronics Engineers, Los Alamitos, CA, 2001, pp. 3986–3991.

[6] Wright, J. R., "Sequential Orbit Determination with Auto-Correlated Gravity Modeling Errors," *Journal of Guidance, Control, and Dynamics*, Vol. 4, No. 2, May–June 1981, pp. 304–309.

[7] Wright, J. R., and Woodburn, J., "Simultaneous Real-time Estimation of Atmospheric Density and Ballistic Coefficient," *Spaceflight Mechanics 2004*, for American Astronautical Society by Univelt, San

Diego, CA, 2004, p. 6; also American Astronautical Society Paper AAS-04-175.

[8] Mitchell, M., Breger, L. S., How, J. P., and Alfriend, K. T., "Effects of Navigation Filter Properties on Formation Flying Control," AIAA Paper 2004-5024, 2004.

[9] Tillerson, M., Inalhan, G., and How, J. P., "Coordination and Control of Distributed Spacecraft Systems Using Convex Optimization Techniques," *International Journal of Robust and Nonlinear Control*, Vol. 12, Nos. 2–3, Feb.–Mar. 2002, pp. 207–242.

[10] Kaplan, M., *Modern Spacecraft Dynamics and Control*, Wiley, New York, 1976, p. 112.

[11] Busse, F. D., "Precise Formation-State Estimation in Low Earth Orbit Using Carrier Differential GPS," Ph.D. Dissertation, Stanford University, Department of Aeronautics and Astronautics, Feb. 2003, p. 5.

[12] Busse, F. D., Simpson, J., and How, J. P., "Demonstration of Adaptive Extended Kalman Filtering for LEO Formation Estimation Using CDGPS," *Journal of the Institute of Navigation*, Vol. 50, No. 2, 2003, pp. 79–94.

[13] Gelb, A., *Applied Optimal Estimation*, MIT Press, Cambridge, MA, 1974, p. 102.

[14] Junkins, J., Akella, M., and Alfriend, K. T., "Non-Gaussian Error Propagation in Orbital Mechanics," *Journal of the Astronautical Sciences*, Vol. 44, No. 4, 1996, p. 541.

[15] Mitchell, M., "CDGPS-Based Relative Navigation for Multiple Spacecraft," S.M. Thesis, Massachusetts Institute of Technology, Department of Aeronautics and Astronautics, June 2004, p. 21.

[16] Franklin, G., Powell, J., and Workman, M., *Digital Control of Dynamic Systems*, 2nd ed., Addison–Wesley, Reading, MA, 1998, p. 53.